

Real-time Dissection and Forecast of Infection Dynamics during a Pandemic

Steven Schulz^{a,*}, Richard Pastor^a, Cenk Koyuncuoglu^a, Forrest W. Crawford^{b,c,d,e}, Detlef Zernick^a, André Karch^f, and Sten Rüdiger^a

^a*Machine Learning and Health Unit, Department of Engineering, NET CHECK GmbH, Berlin, Germany*

^b*Department of Biostatistics, Yale School of Public Health, New Haven, CT, USA*

^c*Department of Statistics and Data Science, Yale University, New Haven, CT, USA*

^d*Department of Ecology and Evolutionary Biology, Yale University, New Haven, CT, USA*

^e*Yale School of Management, New Haven, CT, USA*

^f*Institute of Epidemiology and Social Medicine, Westfälische Wilhelms-Universität Münster, Münster, Germany*

Abstract

Pandemic preparedness requires institutions, including public health authorities and governments, to detect, survey and control outbreaks. To maintain an accurate, quantitative and up-to-date picture of an epidemic crisis is key. For SARS-CoV-2, this was mostly achieved by ascertaining incidence numbers and the effective reproductive number (R_{eff}), which counts how many people an infected person is likely to infect on average. These numbers give strong hints on past infection dynamics in a population but fail to clearly characterize current and future dynamics as well as potential effects of pharmaceutical and non-pharmaceutical interventions. We show that, by using and combining infection surveillance and population-scale contact statistics, we can obtain a better understanding of the drivers of epidemic waves and the effectiveness of interventions. This approach can provide a real-time picture, thus saving not only many lives by quickly allowing adaptation of the health policies but also alleviating economic and other burdens if an intervention proves ineffective. We factorize R_{eff} into contacts and relative transmissibility: Both signals can be used, individually and combined, to identify driving forces of an epidemic, monitoring and assessing interventions, as well as projecting an epidemic's future trajectory. Using data for SARS-CoV-2 and Influenza from 2019 onward in Germany, we provide evidence for the usefulness of our approach. In particular, we find that the effects from physical distancing and lockdowns as well as vaccination campaigns are dominant.

1. Introduction

Infectious diseases represent serious threats to an ever increasingly connected humankind, on par with e.g. natural disasters and infrastructure failures. Epidemic preparedness – the ability to predict and mitigate future epidemic outbreaks – has thus risen to one of the most pressing challenges in modern societies and recently focused a wealth of

research efforts building on a variety of data [1] in response to awareness elicited by the SARS-CoV-2 pandemic [2].

Epidemic dynamics are shaped at the crossroads of human and viral driving forces: a pathogen's reproductive cycle, defining its relative transmission rate upon physical proximity between individuals with full or partial susceptibility, as well as human behaviour, via the frequency of transmission-prone contacts between individuals itself [3]. Critical events such as the emergence of fitter mutants or

*Corresponding author: steven.schulz@netcheck.de.

collective shifts in human activity patterns set the pace for new epidemic waves. Real-time monitoring of these forces during an epidemic, whether it is fueled mostly by increased contact levels or changes in relative transmissibility, is of paramount value for epidemic forecasting as well as the ability to set up informed, targeted mitigation strategies and estimating the effects of (non-)pharmaceutical health policies [4].

Using SARS-CoV-2 and Influenza as key examples of airborne transmissible contagions, we showcase monitoring and forecast tools for epidemic crises centered around a crowdsourcing-based, real-time method to assess levels of physical proximity in a population using GPS location information, the Contact Index CX [5]. We show that diverging trends between contact levels and independently recorded infection surveillance are indicators of altered relative viral transmissibility. Using 2020-specific data as a baseline for purely contact-driven SARS-CoV-2 epidemics, all observed transition points are explained by the onset of key immune escape variants (alpha, delta, omicron). The resulting dual evolution, Contact Index CX and relative transmissibility T , provides a highly transparent and timely picture of ongoing epidemics, including the possibility to identify likely driving forces in future epidemic waves.

2. Materials and Methods

2.1. Contact metrics relevant for epidemics

Contact networks are a representation of human interactions [6] with immediate implications for the spread of contagions in a population [7, 8]. Nodes represent individuals and edges are drawn between pairs of nodes in the event of contact between them (Figure S3(a)). A contagion can propagate through a population along paths following the links of the network.

Intuitively, transmission levels scale with the average number of links per node $\langle k \rangle =$

$\sum_{k \geq 0} kP(k) = 2L/N$ [3], where $P(k)$ is the distribution of these numbers across a network and N (L) is the number of nodes (links). Beyond this local property, more global topological network features – how contacts are collectively configured across the network – do also affect the course of epidemics [3] by fueling and constraining the number of available paths. Groundbreaking epidemiological and network-theoretical work established that the effective reproduction number R_{eff} , quantifying epidemic spreading, scales with $\frac{\langle k^2 \rangle}{\langle k \rangle}$ [3, 9, 10, 11, 12], i.e. the presence of very social nodes (superspreaders) with outstanding k mediate enhanced propagation. Typical social networks are very inhomogeneous in terms of social activity, with outstanding community structure and few individuals responsible for most contacts [9]. The pivotal role of the second moment $\langle k^2 \rangle = \sum_{k \geq 0} k^2 P(k)$ is intuited by the *friendship paradox* [13]: An individual’s friends are on average more social than oneself; in other words, the number of next-nearest neighbors $\langle k^2 \rangle$ in the network exceeds the expectation $\langle k \rangle^2$ from the number of nearest neighbors, a mere consequence of non-zero variance in $P(k)$: $\langle k^2 \rangle - \langle k \rangle^2 > 0$.

2.2. Assessing contact levels in real-world networks

The contact network relevant to transmission of airborne viruses such as Influenza and SARS-CoV-2 arises from physical proximity between individuals. Compared to (virtual) social networks, such real-world networks are expected to have distinct properties, as they are constrained by geography and physical distance, but are also tremendously more difficult to track at the population scale. Coarse contact and mixing patterns in real-world networks have been inferred using limited data gathered from surveys [14, 15] or viral phylogeny [16]. Locally confined real-world networks, such as on cruise ships [17], school campuses [18] or within towns [19] have been measured using Bluetooth communication between nearby mobile devices.

We use a previously developed approach to probe population-scale real-world contact networks based on crowdsourced datasets of GPS locations [20, 5] to measure the Contact Index $CX = \frac{\langle k^2 \rangle}{\langle k \rangle}$ as a statistical measure of contact levels relevant for epidemics [5]. The crowdsourcing data is collected in near real-time via opt-in from each of an anonymized panel of 1 million mobile app users (roughly 1% of Germany’s population) and consists of ≈ 100 daily samples per device tagged with time and GPS location information. It allows us to reconstruct samples of the actual contact network realized in the population: Contacts (links) are drawn between devices (nodes) co-located in space and time (Supp Mat S1).

2.3. Network sampling correction

The incomplete nature of such crowdsourced data represents a major challenge: Contacts from uninvolved or inactive devices are not captured, giving rise to missing nodes and links in the network. This aspect of our data can be crafted into a network sampling framework [21, 22] in which nodes and edges are randomly removed with probabilities p and q , respectively (Figure S3(a,b) and Supp Mat S2). These sampling parameters also change over time, mostly in response to software updates and app usage, and are heterogeneous in space. Our improved mathematical modeling based on Horvitz-Thompson theory disentangles actual changes in contact levels from signals unrelated to the users’ contact behaviour, thus achieving persistent and comparable results across the full time span since the beginning of measurement in 2019 (Supp Mat S2 and Supp Mat S3).

Importantly, abstractions of contact networks exist in two distinct flavours: weighted versus unweighted [23]. Links may be endowed with weights $w_{ij} \in \{0, 1, 2, \dots\}$ representing the duration or multiplicity of contact between individuals i and j [24] or simply indicate the presence or absence of contact $a_{ij} = \text{sgn}(w_{ij}) \in \{0, 1\}$ (Figure S3(c)). In

the epidemiological context, we assume that network topology, represented by a_{ij} , is more important than the recurrence of contacts between the same individuals: For instance, the (statistical) contribution to viral spread from a cluster of short contacts at a crowded event would outpace a lengthy contact between an isolated couple while in lockdown. We thus focus on unweighted networks and exclude contact duration in our analyses other than in the fact that short contacts are unlikely to be recorded during the random sampling inherent to the crowdsourcing method.

However, network sampling destroys topological information about underlying complete networks (Figure S3(c)); the success of Horvitz-Thompson theory [21] to establish a connection between original and sample networks relies in the use of weighted links. To establish the same connection for unweighted networks, we devised a Bayesian framework which encodes missing topological information as a prior weight distribution $P(w|w > 0)$ (Supp Mat S2). We find that available complete real-world networks in various contexts [17, 18, 19] appear to show strikingly similar weight distributions (Figure S3(d)), which suggests a universal shape of $P(w|w > 0)$ also applicable to our problem. These distributions are consistent with power laws with small exponents [25, 26], a repeatedly demonstrated feature of complex networks [27] and beyond [28]. Yet, we do not imply that power laws are the true mechanism behind network weights, as a variety of other distribution classes are easily confounded with power laws [28, 29, 30].

3. Results

3.1. Evolution of CX since 2019

By means of our refined correction method for network sampling effects, we achieve a consistent measurement of contact levels since the beginning of crowdsourcing in 2019, despite the time-dependent sampling. That is, we cover the prelude

181 and entire course of the SARS-CoV-2 epidemic in
182 Germany (Figure 1(a)). The gap in February 2020
183 is explained by missing data due to the rollout of a
184 major crowdsourcing software update.

185 Holiday season comes along with reduced CX un-
186 der normal conditions, as shown by the Fall and
187 Christmas breaks in 2019, thus showing a reduction
188 of transmission-prone contacts. The onset of the
189 first SARS-CoV-2 wave in March 2020 induced an
190 unequivocally more pronounced drop in CX , prob-
191 ably explained by a more systematic cessation of
192 super-spreading activities.

193 Since onset of the SARS-CoV-2 pandemic,
194 changes in contact behaviour as reflected by CX
195 underwent several periods of spiking (partial or
196 complete deregulation of mass events in fall 2020,
197 fall 2021 and spring 2022) and damping (winter
198 wave 2020, emergence of the omicron variant in
199 late 2021). Overall, a similar evolution is observed
200 between CX and the rigor of SARS-CoV-2-related
201 policy as measured by the Government-Response
202 Index [31] (Figure S1(a)), thus indicating broad
203 awareness of the situation at the population and
204 governance levels albeit no causal link shall be im-
205 plied.

206 Interestingly, recent CX values have not yet re-
207 turned to pre-pandemic levels by a factor of 2 to 3,
208 despite a return to no contact-related restrictions
209 in 2022. This suggests the existence of a hystere-
210 sis effect in addition to the fast response of CX
211 discussed above: The collective behaviour has not
212 returned to its unperturbed state in response to re-
213 laxed conditions, possibly as a result of continued
214 broad perception of disease risk [32, 33].

215 From a dimensional viewpoint, CX represents
216 an average number of (next-nearest) contacts per
217 (nearest) contact: Comparing values of CX across
218 areas with vastly different population densities
219 within Germany supports our expectation that CX
220 scales (non-linearly) with the absolute propensity
221 of physical proximity between individuals (Fig-

222 ure S4(d) and Supp Mat S3).

223 3.2. Deciphering epidemic forces: contacts vs. rel- 224 ative transmissibility

225 In 2020, SARS-CoV-2 epidemic trends were pri-
226 marily driven by trends in contact levels, as both
227 immune escape variants and vaccines were not yet
228 relevant and relative SARS-CoV-2 transmissibility
229 – its intrinsic transmission probability per contact
230 – was thus constant (Figure 1(b)): Official daily
231 now-cast reproduction numbers R_{eff} , independently
232 recorded from national infection surveillance [34],
233 correlate well with daily CX , but CX shows a
234 time lead of approximately 2 – 3 weeks over R_{eff}
235 (Figure S1(a, right inset)) [5], explained by incu-
236 bation time as well as testing and reporting de-
237 lays. This underlines the predictive character of
238 real-time contact metrics for wild-type dominated
239 epidemics [20]. Since then, the correlation between
240 R_{eff} and CX has repeatedly changed, with the re-
241 sulting signal quantifying shifts in relative transmis-
242 sibility accountable to key epidemic changes other
243 than contacts.

244 The effective reproduction number R_{eff} is defined
245 by $R_{\text{eff}} = \langle k \rangle \cdot U \cdot \tau$, where $\langle k \rangle$ denotes the contact
246 number per day, U the probability of transmission
247 per contact, and τ the mean duration of infectivity
248 in days. Both U and τ are determined by physio-
249 logical processes involved in transmission and, to-
250 gether, define the intrinsic transmission efficiency
251 (per contact) $T = U \cdot \tau$.

252 Furthermore, as we assume $CX = \frac{\langle k^2 \rangle}{\langle k \rangle}$
253 replaces $\langle k \rangle$, we replace the definition by
254 $R_{\text{eff}} = (a + b \cdot CX) \cdot T$. A linear relationship of
255 this form between CX and R_{eff} is motivated by our
256 findings in 2020. We use values for a and b obtained
257 from a linear regression between CX and wild-type
258 R_{eff} data at the optimal time delay of $\Delta t = 16$ days
259 (Figure S1(a, left inset) and Supp Mat S4). Upon
260 interpreting $R_{\text{WT}}(CX) \equiv a + b \cdot CX$ as the wild-type

specific reproduction number, we have that

$$R_{\text{eff}} = R_{\text{WT}}(CX) \cdot T, \quad (1)$$

where T represents relative transmissibility with respect to wild-type in a fully susceptible population ($T_{\text{WT}} = 1$). Note that, in contrast to now-cast data, Eq. (1) assigns reproduction numbers to the day of contact/infection.

From independently recorded values for R_{eff} and CX , we can determine the relative transmissibility of the contagion by factoring out contact-related contributions from overall infection dynamics as $T = \frac{R_{\text{eff}}}{R_{\text{WT}}(CX)}$ for any given day. We expect network-wide propagation of transmissibility-related information to be slow compared to network dynamics itself and, thus, T to undergo evolution on longer timescales. We interpret fast signal in T as random fluctuations from the measurement of R_{eff} and capture actual trends by $\langle T \rangle$, centered averages over sliding time windows of 2 months (Supp Mat S4).

3.3. Epidemic evolution of relative SARS-CoV-2 transmissibility

The evolution of relative SARS-CoV-2 transmissibility $\langle T \rangle$ is shown in Figure 1(b). This time series reenacts the various phases of the SARS-CoV-2 pandemic:

Relative SARS-CoV-2 transmissibility $\langle T \rangle$ is approximately equal to unity throughout 2020, an initial period purely driven by unperturbed wild-type epidemics that we used to “calibrate” CX and R_{eff} which evolve on shorter timescales. It subsequently follows a tug-of-war pattern shaped by alternating epidemic forces beyond contacts: immune escape variants and development of population immunity through infection and vaccination. Three waves of increased relative transmissibility are explained by the takeover of fitter virus lineages (Figure 1(b)), specifically alpha (spring 2021), delta (summer 2021) and omicron BA.1/BA.2 (win-

ter 2021/22). We hypothesize that subsequent relaxation of $\langle T \rangle$ after each wave may be attributed to natural immunity, while the superposed long-term downward trend may be explained by the additional immunity acquisition through (initial and booster) vaccination campaigns. Interestingly, the effect of omicron BA.4/BA.5 takeover in summer 2022 on $\langle T \rangle$ is nowhere close to those of previous variants.

Comparing correlations with different parameters rules out the possibility that the measured $\langle T \rangle$ is shaped by factors confounding the reproduction numbers or CX values (Figure S1(b,c) and Supp Mat S4). These possible confounders include viral prevalence, CX itself through higher-order effects from network sampling not captured by our modeling and other topological network features (such as clustering, small-world properties) as well as R_{eff} itself through changes in testing strategies and systematic under-reporting of infections [35]. For instance, testing individuals indiscriminately versus focusing test capacities on suspected infection cases may lead to incomparable snapshots of ongoing infection dynamics. Overall, strong positive correlation is exclusively observed between $\langle T \rangle$ and variant dynamics (Figure S1(b,c)) [36]. In this analysis, we use test positivity [37] and results from local prevalence studies [38] as proxies for overall prevalence. Also, we neglect possible effects from network sampling on different topological measures [39, 40], but we expect trends to be conserved as long as the sampling process remains unchanged.

We note the absence of seasonal oscillations in $\langle T \rangle$ as well as clear signatures of mask mandates (in effect across many social contexts between April 2020 and April 2022). A seasonal oscillation in $\langle T \rangle$, larger values in winter and smaller values in summer, might be expected from the shift of human activity between in- and outdoor settings. Also, previous research established the effectiveness of mask usage at reducing transmission of respiratory diseases (reviewed in [41]). Overall, our results sug-

340 gest that, at least in the epidemic stage of SARS-
341 CoV-2, infection rates were predominantly driven
342 by the strong variability in contacts as well as the
343 repeated emergence of more transmissible variants,
344 in line with previous findings [42, 43, 44].

345 3.4. Forecast of infection level and trend changes

346 The challenge of epidemic forecast consists in the
347 accurate prediction of current and future reproduc-
348 tion numbers R_{eff} . Using the rationale that trends
349 in infection levels carry the combined signature of
350 trends in contact and relative transmissibility lev-
351 els, we propose to construct predictions according
352 to

$$R_{\text{true}}(t) = R_{\text{WT}}(CX(t)) \cdot \langle T(t) \rangle, \quad (2)$$

353 where R_{true} is assigned to the projected day of con-
354 tact/infection. The key difference to Eq. (1) is the
355 use of $\langle T \rangle$ which eliminates noise from reproduc-
356 tion numbers. Importantly, we therefore expect
357 that our prediction R_{true} represents actual epidemic
358 trends (ground truth) more accurately than epi-
359 demic surveillance (R_{eff}).

360 Figure 1(c) shows R_{true} together with data from
361 infection surveillance, both plotted with respect to
362 their date of recording (assuming real-time CX
363 measurement). This shows how our prediction
364 overall anticipates current epidemic trends that
365 are observed via infection surveillance only about
366 $\Delta t = 2 - 3$ weeks later. Thus, we propose to use
367 our method as a tool for real-time infection surveil-
368 lance.

369 To extend forecasts beyond this horizon and pre-
370 dict future reproduction numbers, CX and $\langle T \rangle$
371 themselves need to be projected beyond latest data.
372 For several choices of the current day t_0 , Figure 2(a)
373 showcases forecasts (R_{pred}) where CX and $\langle T \rangle$ are
374 continued beyond the last days of available data
375 (t_0 and $t_0 - \Delta t$, respectively) using autoregressive
376 integrated moving average (ARIMA) models prior
377 to applying Eq. (2) (Supp Mat S5). These fore-

378 casts outperform a null forecast based on a mere
379 ARIMA-type continuation of infection surveillance
380 data (R_{eff}), as shown by narrower distributions of
381 residuals ($R_{\text{pred}} - R_{\text{true}}$) across all choices of t_0 (Fig-
382 ure 2(a)). Furthermore, we highlight the broad ap-
383 plicability of our method to airborne infectious dis-
384 eases by performing an identical forecast analysis
385 for Influenza (Figure S2(a)), using coarser infection
386 surveillance data [45] and presuming a similar rela-
387 tionship between R_{eff} and CX as for SARS-CoV-2
388 (Supp Mat S5).

389 Most importantly, trend changes in epidemic
390 driving forces such as $\langle T \rangle$ and CX are indicators of
391 new phases in an epidemic. Timely detection of new
392 trends in these time series, e.g. using anomaly de-
393 tection methods, can provide valuable information
394 to estimate the risk of upcoming epidemic waves
395 and to predict their nature – whether dynamics is
396 fueled by contacts or increased transmission effi-
397 ciency. Such trend detection is potentially easier
398 to achieve but equally informative than the abil-
399 ity to accurately predict infection surveillance. The
400 onset of rising trends could shape decision-making
401 with regard to the effectiveness of health policies,
402 e.g. pharmaceutical and non-pharmaceutical in-
403 terventions for rising $\langle T \rangle$ and CX , respectively.
404 Figures 2(b) and S2(b) highlight rising and falling
405 trends in both CX and T for SARS-CoV-2 and In-
406 fluenza, respectively, akin to trends in stock prices.
407 For SARS-CoV-2, trend changes are timely indica-
408 tors of all major escape variant- and contact-driven
409 epidemic turning points (Figure 2(b)). Unlike for
410 SARS-CoV-2 in its epidemic stage, major upheavals
411 in relative transmissibility for Influenza are limited
412 to seasonality, with the notable exception of 2020,
413 presumably reflecting its endemic dynamics (Fig-
414 ure S2(b)).

415 4. Conclusion

416 We presented a simple, yet insightful quantitative
417 method for a data-driven decomposition of overall

418 epidemic dynamics into contact-related and trans- 459
419 mission efficiency-related contributions. It relies on 460
420 both the availability of infection surveillance data 461
421 as well as crowdsourced GPS location data to detect 462
422 and quantify physical proximity between suscepti- 463
423 ble individuals. Its appeal resides in the merely 464
424 bivariate yet highly informative projection of epi- 465
425 demics paving the way towards timely identifica- 466
426 tion of driving forces in an ongoing epidemic – hu- 467
427 man versus viral factors – and possibly effective 468
428 mitigation strategies – pharmaceutical versus non- 469
429 pharmaceutical.

430 The approach can be used for epidemic forecast 471
431 in multiple ways. Recent and projected future val- 472
432 ues of CX and $\langle T \rangle$ can be used for short-term 473
433 ($2 - 3$ weeks) and long-term prediction of infection 474
434 or reproduction numbers, thus taking our previ- 475
435 ously described short-term forecast further [5]. Yet, 476
436 a timely detection of trend changes could reliably 477
437 forecast upcoming waves and their nature without 478
438 the necessity to accurately predict infection surveil- 479
439 lance data. These tools can lead towards a more 480
440 strategic approach to epidemic mitigation and po- 481
441 tentially save lives by reducing the spread of deadly 482
442 diseases.

443 Results from the presumably most systematically 484
444 tracked epidemic to date, SARS-CoV-2, draw the 485
445 picture of co-evolution within the virus-host rela- 486
446 tion: Increasing immunity levels in the host pop- 487
447 ulation alternate with step-wise adaptation of the 488
448 virus through immune-escape variants. Other fre- 489
449 quently discussed factors, including mask policies 490
450 and seasonality, are presumably still below the cur- 491
451 rent statistical resolution of our method, defined by 492
452 the sampling noise in the CX and R_{eff} time series.
453 Moreover, a larger impact of seasonal variation is
454 expected in the endemic phase of SARS-CoV-2 [46].

455 Our method is broadly applicable to airborne 494
456 contagions beyond SARS-CoV-2, but depends on 495
457 the availability of infection surveillance and crowd- 496
458 sourcing strategies that remain persistent over ex- 497

tended amounts of time. Changes in testing strat-
egy can lead to signal and biases unrelated to un-
derlying epidemic driving forces [35]. More cru-
cially, systematic infection surveillance is not im-
plemented beyond the case of SARS-CoV-2. We
illustrated a framework to correct for the effect
of varying sampling depth in the contact network.
Yet, higher-order effects in the signal can occur as
a result of sampling aspects not captured by our
mathematical modeling. In order to ensure valid
prognoses through our method, we advocate for sys-
tematic and persistent crowdsourcing and infection
surveillance strategies across a variety of diseases
with epidemic potential.

Geographical resolution of our forecast method
is currently limited by the sampling depth, as the
estimation especially of higher moments of degree
distributions $P(k)$ becomes increasingly difficult as
smaller portions of the network are available. A
higher spatial resolution of contact and relative
transmissibility levels, with potential to locate the
origin of new variants of concern and define locally
targeted mitigation strategies, can be achieved by
e.g. increasing the panel of app users.

Our analysis assumes statics, but actual contact
networks are dynamic in nature [47, 48]: While
some contacts are frequently repeated (e.g. be-
tween household members), other contacts are ran-
domly redrawn on each occasion (e.g. in pub-
lic transportation), with implications for epidemic
spread [49, 50]. Our method can be improved by
analyzing contact data in light of existing models
of dynamic networks [51, 48].

492 Acknowledgment

493 This work was supported by grants from the
494 Federal Government of Germany through the
495 Federal Ministry for Economic Affairs and Cli-
496 mate Action (BMWK) for the project DAKI-FWS
497 (01MK21009A) and the Federal Ministry of Educa-

498 tion and Research (BMBF) for the project Optim-
499 Agent (031L0299).

500 References

- 501 [1] A. Rodríguez, H. Kamarthi, P. Agarwal, J. Ho, M. Pa-
502 tel, S. Sapre, B. A. Prakash, Data-centric epidemic
503 forecasting: A survey, arXiv preprint arXiv:2207.09370
504 (2022).
- 505 [2] A. Maxmen, Has covid taught us anything about pan-
506 demic preparedness?, *Nature* (2021) 332–335.
- 507 [3] R. Pastor-Satorras, C. Castellano, P. Van Mieghem,
508 A. Vespignani, Epidemic processes in complex net-
509 works, *Reviews of modern physics* 87 (3) (2015) 925.
- 510 [4] T. Alamo, D. G. Reina, P. M. Gata, V. M. Preciado,
511 G. Giordano, Data-driven methods for present and fu-
512 ture pandemics: Monitoring, modelling and managing,
513 *Annual Reviews in Control* 52 (2021) 448–464.
- 514 [5] S. Rüdiger, S. Konigorski, A. Rakowski, J. A. Edelman,
515 D. Zernick, A. Thieme, C. Lippert, Predicting the sars-
516 cov-2 effective reproduction number using bulk contact
517 data from mobile phones, *Proceedings of the National*
518 *Academy of Sciences* 118 (31) (2021).
- 519 [6] M. E. Newman, J. Park, Why social networks are dif-
520 ferent from other types of networks, *Physical review E*
521 68 (3) (2003) 036122.
- 522 [7] M. Keeling, The implications of network structure
523 for epidemic dynamics, *Theoretical population biology*
524 67 (1) (2005) 1–8.
- 525 [8] C. Moore, M. E. Newman, Epidemics and percolation in
526 small-world networks, *Physical Review E* 61 (5) (2000)
527 5678.
- 528 [9] M. Barthélemy, A. Barrat, R. Pastor-Satorras,
529 A. Vespignani, Dynamical patterns of epidemic out-
530 breaks in complex heterogeneous networks, *Journal of*
531 *theoretical biology* 235 (2) (2005) 275–288.
- 532 [10] Y. Moreno, R. Pastor-Satorras, A. Vespignani, Epi-
533 demic outbreaks in complex heterogeneous networks,
534 *The European Physical Journal B-Condensed Matter*
535 *and Complex Systems* 26 (4) (2002) 521–529.
- 536 [11] R. M. May, R. M. Anderson, The transmission dynam-
537 ics of human immunodeficiency virus (hiv), *Philosophical*
538 *Transactions of the Royal Society of London. B,*
539 *Biological Sciences* 321 (1207) (1988) 565–607.
- 540 [12] R. M. May, R. M. Anderson, Commentary transmission
541 dynamics of hiv infection, *Nature* 326 (137) (1987) 10–
542 1038.
- 543 [13] S. L. Feld, Why your friends have more friends than you
544 do, *American journal of sociology* 96 (6) (1991) 1464–
545 1477.
- 546 [14] J. M. Read, K. T. Eames, W. J. Edmunds, Dynamic
547 social networks and the implications for the spread of
548 infectious disease, *Journal of The Royal Society Inter-*
549 *face* 5 (26) (2008) 1001–1007.
- 550 [15] J. Mossong, N. Hens, M. Jit, P. Beutels, K. Auranen,
551 R. Mikolajczyk, M. Massari, S. Salmaso, G. S. Tomba,
552 J. Wallinga, et al., Social contacts and mixing pat-
553 terns relevant to the spread of infectious diseases, *PLoS*
554 *medicine* 5 (3) (2008) e74.
- 555 [16] G. E. Leventhal, R. Kouyos, T. Stadler, V. Von Wyl,
556 S. Yerly, J. Böni, C. Celleraï, T. Klimkait, H. F.
557 Günthard, S. Bonhoeffer, Inferring epidemic contact
558 structure from phylogenetic trees, *PLoS computational*
559 *biology* 8 (3) (2012) e1002413.
- 560 [17] R. Pung, J. A. Firth, L. G. Spurgin, V. J. Lee, A. J.
561 Kucharski, Using high-resolution contact networks to
562 evaluate sars-cov-2 transmission and control in large-
563 scale multi-day events, *Nature communications* 13 (1)
564 (2022) 1–11.
- 565 [18] P. Sapiezynski, A. Stopczynski, D. D. Lassen,
566 S. Lehmann, Interaction data from the copenhagen net-
567 works study, *Scientific Data* 6 (1) (2019) 1–10.
- 568 [19] S. M. Kissler, P. Klepac, M. Tang, A. J. Conlan, J. R.
569 Gog, Sparking “the bbc four pandemic”: Leveraging
570 citizen science and mobile phones to model the spread
571 of disease, *BioRxiv* (2020) 479154.
- 572 [20] F. W. Crawford, S. A. Jones, M. Cartter, S. G. Dean,
573 J. L. Warren, Z. R. Li, J. Barbieri, J. Campbell, P. Ken-
574 ney, T. Valleau, et al., Impact of close interpersonal
575 contact on covid-19 incidence: Evidence from 1 year
576 of mobile device data, *Science Advances* 8 (1) (2022)
577 eabi5499.
- 578 [21] E. D. Kolaczyk, G. Csárdi, *Statistical analysis of net-*
579 *work data with R*, Vol. 65, Springer, 2014.
- 580 [22] P. Hu, W. C. Lau, A survey and taxonomy of graph
581 sampling, arXiv preprint arXiv:1308.5865 (2013).
- 582 [23] M. Á. Serrano, M. Boguñá, R. Pastor-Satorras, Corre-
583 lations in weighted networks, *Physical Review E* 74 (5)
584 (2006) 055101.
- 585 [24] A. Barrat, M. Barthelemy, R. Pastor-Satorras,
586 A. Vespignani, The architecture of complex weighted
587 networks, *Proceedings of the national academy of sci-*
588 *ences* 101 (11) (2004) 3747–3752.
- 589 [25] H. Ebel, L.-I. Mielsch, S. Bornholdt, Scale-free topol-
590 ogy of e-mail networks, *Physical review E* 66 (3) (2002)
591 035103.
- 592 [26] M. E. Newman, Scientific collaboration networks. i. net-
593 work construction and fundamental results, *Physical re-*
594 *view E* 64 (1) (2001) 016131.
- 595 [27] R. Guimera, S. Mossa, A. Turtleschi, L. N. Amaral,
596 The worldwide air transportation network: Anoma-
597 lous centrality, community structure, and cities’ global
598 roles, *Proceedings of the National Academy of Sciences*
599 102 (22) (2005) 7794–7799.

- 600 [28] A. Clauset, C. R. Shalizi, M. E. Newman, Power-law 652
601 distributions in empirical data, *SIAM review* 51 (4) 653
602 (2009) 661–703. 654
- 603 [29] J.-D. J. Han, D. Dupuy, N. Bertin, M. E. Cusick, 655
604 M. Vidal, Effect of sampling on topology predictions 656
605 of protein-protein interaction networks, *Nature biotechnol-* 657
606 *ogy* 23 (7) (2005) 839–844. 658
- 607 [30] R. Perline, Strong, weak and false inverse power laws, 659
608 *Statistical Science* (2005) 68–88. 660
- 609 [31] T. Hale, N. Angrist, R. Goldszmidt, B. Kira, A. Pether- 661
610 ick, T. Phillips, S. Webster, E. Cameron-Blake, L. Hal- 662
611 las, S. Majumdar, et al., A global panel database of pan- 663
612 demic policies (oxford covid-19 government response 664
613 tracker), *Nature human behaviour* 5 (4) (2021) 529– 665
614 538. 666
- 615 [32] C. Betsch, S. Eitze, P. Sprengholz, L. Korn, P. Sham- 667
616 srizi, M. Geiger, E. Sievert, L. Lehrer, M. Jenny, Zusan- 668
617 menfassung und empfehlungen welle 69 (2022). 669
618 URL [https://projekte.uni-erfurt.de/cosmo2020/](https://projekte.uni-erfurt.de/cosmo2020/web/summary/69/) 670
619 [web/summary/69/](https://projekte.uni-erfurt.de/cosmo2020/web/summary/69/) 671
- 620 [33] C. Betsch, L. Wieler, M. Bosnjak, M. Ramharter, 672
621 V. Stollorz, S. Omer, L. Korn, P. Sprengholz, L. Fel- 673
622 gendreff, S. Eitze, P. Schmid, Germany covid-19 snap- 674
623 shot monitoring (cosmo germany): Monitoring knowl- 675
624 edge, risk perceptions, preventive behaviours, and pub- 676
625 lic trust in the current coronavirus outbreak in germany 677
626 (Mar. 2020). doi:10.23668/psycharchives.2776. 678
627 URL [https://psycharchives.org/index.php/en/](https://psycharchives.org/index.php/en/item/e5acdc65-77e9-4fd4-9cd2-bf6aa2dd5eba) 679
628 [item/e5acdc65-77e9-4fd4-9cd2-bf6aa2dd5eba](https://psycharchives.org/index.php/en/item/e5acdc65-77e9-4fd4-9cd2-bf6aa2dd5eba) 680
- 629 [34] M. an der Heiden, Sars-cov-2-nowcasting und -r- 681
630 schaetzung (Jan. 2023). doi:10.5281/zenodo.7571376. 682
631 URL <https://doi.org/10.5281/zenodo.7571376> 683
- 632 [35] H. Rossman, E. Segal, Nowcasting the spread of sars- 684
633 cov-2, *Nature microbiology* 7 (1) (2022) 16–17. 685
- 634 [36] R. Koch-Institut. [link]. 686
635 URL [https://www.rki.de/DE/Content/InfAZ/](https://www.rki.de/DE/Content/InfAZ/N/Neuartiges_N_Coronavirus/Daten/VOC_VOI/_Voi_Tabelle.xlsx?__blob=publicationFile) 687
636 [N/Neuartiges_N_Coronavirus/Daten/VOC_VOI/](https://www.rki.de/DE/Content/InfAZ/N/Neuartiges_N_Coronavirus/Daten/VOC_VOI/_Voi_Tabelle.xlsx?__blob=publicationFile) 688
637 [_Voi_Tabelle.xlsx?__blob=publicationFile](https://www.rki.de/DE/Content/InfAZ/N/Neuartiges_N_Coronavirus/Daten/VOC_VOI/_Voi_Tabelle.xlsx?__blob=publicationFile) 689
- 638 [37] E. Mathieu, H. Ritchie, L. Rodés-Guirao, C. Ap- 690
639 pel, C. Giattino, J. Hasell, B. Macdonald, S. Dat- 691
640 tani, D. Beltekian, E. Ortiz-Ospina, M. Roser, 692
641 Coronavirus pandemic (covid-19), *Our World in* 693
642 *Data*<https://ourworldindata.org/coronavirus> (2020). 694
- 643 [38] H. Neuhauser, N. Buttman-Schweiger, J. Fiebig, 695
644 C. Poethko-Müller, F. Prütz, G. Sarganas Margolis, 696
645 R. Thamm, M. Zimmermann, Observatorium serolo-
646 gischer Studien zu SARS-CoV-2 in Deutschland (Sep.
647 2022). doi:10.5281/zenodo.7043025.
648 URL <https://doi.org/10.5281/zenodo.7043025>
- 649 [39] J. D. Noh, Percolation transition in networks with
650 degree-degree correlation, *Physical Review E* 76 (2)
651 (2007) 026116.
- [40] S. H. Lee, P.-J. Kim, H. Jeong, Statistical properties
of sampled networks, *Physical review E* 73 (1) (2006)
016102.
- [41] J. T. Brooks, J. C. Butler, Effectiveness of mask wear-
ing to control community spread of sars-cov-2, *Jama*
325 (10) (2021) 998–999.
- [42] F. Balloux, C. Tan, L. Swadling, D. Richard, C. Jenner,
M. Maini, L. van Dorp, The past, current and future
epidemiological dynamic of sars-cov-2, *Oxford open im-*
munology 3 (1) (2022) iqac003.
- [43] G. P. Guy Jr, F. C. Lee, G. Sunshine, R. McCord,
M. Howard-Williams, L. Kompaniyets, C. Dunphy,
M. Gakh, R. Weber, E. Sauber-Schatz, et al., Asso-
ciation of state-issued mask mandates and allowing on-
premises restaurant dining with county-level covid-19
case and death growth rates—united states, march 1–
december 31, 2020, *Morbidity and Mortality Weekly*
Report 70 (10) (2021) 350.
- [44] D. K. Chu, E. A. Akl, S. Duda, K. Solo, S. Yaa-
coub, H. J. Schünemann, A. El-Harakeh, A. Bognanni,
T. Lotfi, M. Loeb, et al., Physical distancing, face
masks, and eye protection to prevent person-to-person
transmission of sars-cov-2 and covid-19: a system-
atic review and meta-analysis, *The lancet* 395 (10242)
(2020) 1973–1987.
- [45] R. Koch-Institut, *Survstat@rki* 2.0.
URL <https://survstat.rki.de/>
- [46] J. P. Townsend, A. D. Lamb, H. B. Hassler, P. Sah,
A. A. Nishio, C. Nguyen, A. D. Tew, A. P. Galvani,
A. Dornburg, Projecting the seasonality of endemic
covid-19, *medRxiv* (2022) 2022–01.
- [47] V. Sekara, A. Stopczynski, S. Lehmann, Fundamental
structures of dynamic social networks, *Proceedings of*
the national academy of sciences 113 (36) (2016) 9977–
9982.
- [48] P. Holme, J. Saramäki, Temporal networks, *Physics re-*
ports 519 (3) (2012) 97–125.
- [49] J. Enright, R. R. Kao, Epidemics on dynamic networks,
Epidemics 24 (2018) 88–97.
- [50] E. Valdano, L. Ferreri, C. Poletto, V. Colizza, Analyti-
cal computation of the epidemic threshold on temporal
networks, *Physical Review X* 5 (2) (2015) 021005.
- [51] X. Zhang, C. Moore, M. E. Newman, Random graph
models for dynamic networks, *The European Physical*
Journal B 90 (10) (2017) 1–14.

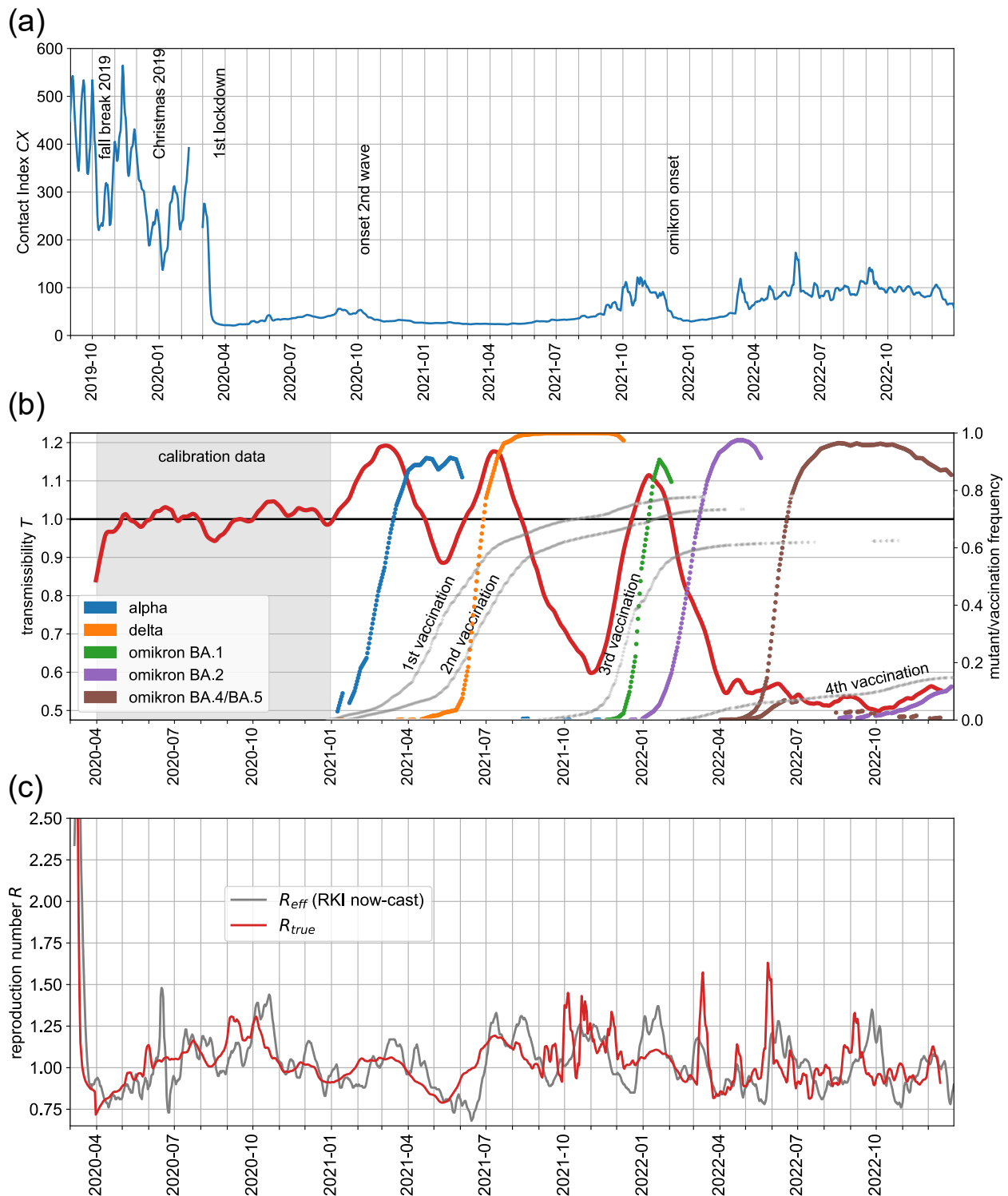


Figure 1: Real-time observation of driving forces in SARS-CoV-2 epidemics: contact levels and relative transmissibility. (a) Evolution of the Contact Index $CX = \langle k^2 \rangle / \langle k \rangle$ in Germany over the course of > 3 years (2019-2022), carrying the signature of various collective behaviour changes in response to the epidemic situation (as indicated). The gap in February 2022 is explained by a major app update. (b) The slowly varying relative transmissibility $\langle T \rangle(t)$ (red) quantifying the intrinsic efficiency of SARS-CoV-2 transmission, measured from the ratio of reproduction numbers (R_{eff}) and contact levels (CX), see Eq. (1). The gray-shaded time interval is wild-type dominated and was used to calibrate CX from our crowdsourcing method and R_{eff} from infection surveillance (Figure S1(a), inset)). The rising frequencies of key SARS-CoV-2 immune escape variants (colored lines, see legend) and well as of vaccine status in Germany (light gray lines) are shown (right axis). (c) Comparison of SARS-CoV-2 effective reproduction numbers R_{eff} from infection surveillance (gray) and projected R_{true} using Eq. (2) (red). All reproduction numbers are assigned to their day of recording.

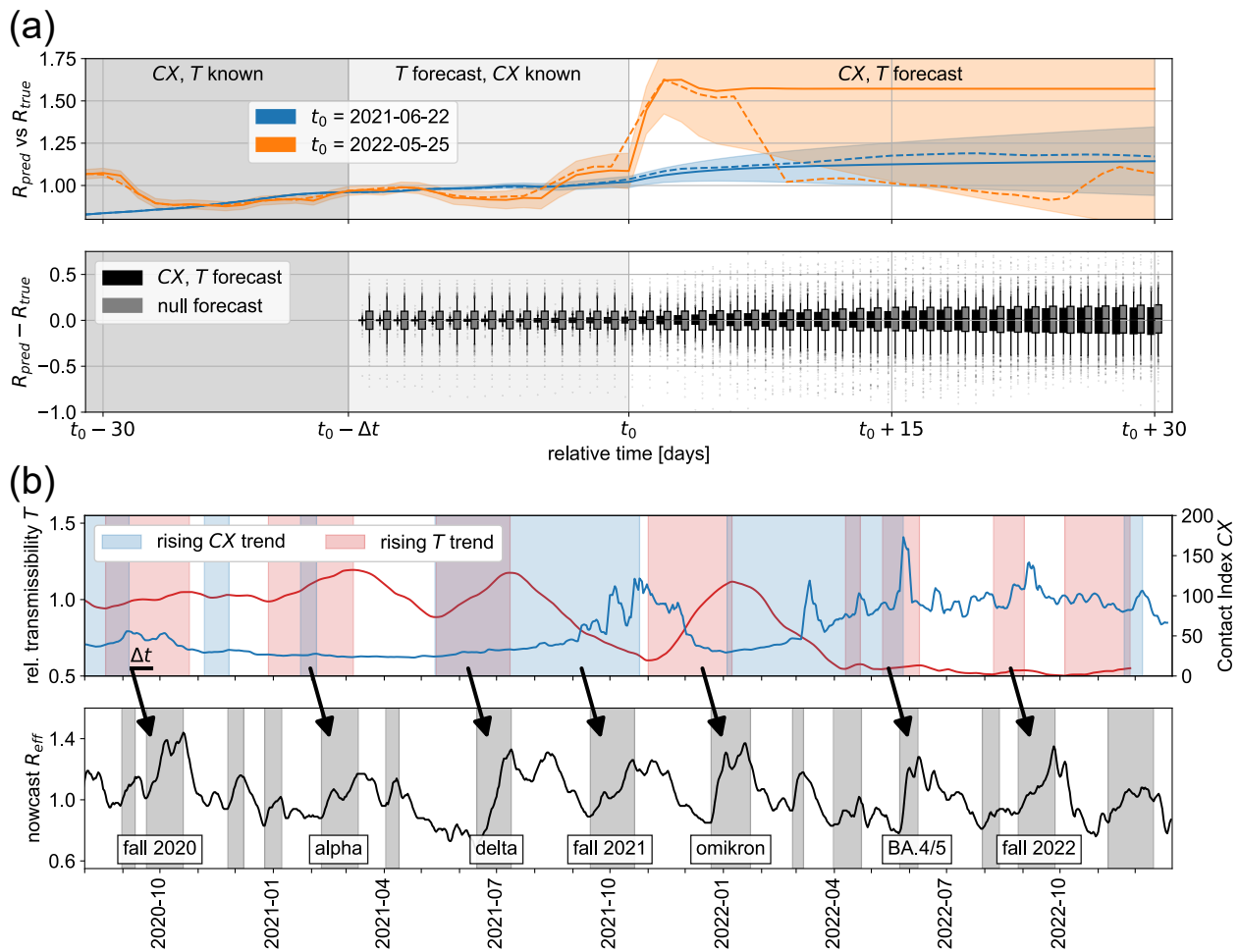


Figure 2: **Forecast of reproduction numbers and trends from contact and transmission efficiency levels.** **(a, upper panel)** Forecast R_{pred} of current and future SARS-CoV-2 reproduction numbers and their uncertainties (solid lines and shaded bands, respectively) using Eq. (2) and the CX and $\langle T \rangle$ time series. Comparison with actual R_{true} values (dashed lines). Denoting the current day by t_0 , R_{eff} and $\langle T \rangle$ are available up to $t_0 - \Delta t$, while CX is near real-time (available up to t_0); the time series are projected beyond their last time points using ARIMA models. The forecast is shown for different choices of the current day t_0 (see legend). **(a, lower panel)** The distribution of residuals between forecasted R_{pred} and actual R_{true} values over all choices of t_0 over the course of 2 years (black box plots). Comparison to residuals from null projections of R_{eff} that make no use of CX (gray box plots), i.e. simple ARIMA model-based projection of infection surveillance data. The boxes indicate quartiles, while whiskers cover 90% of the data. **(b)** Identification of rising trends in both contact levels and transmission efficiency (upper panel) and their relation to rising trends in R_{eff} (lower panel).